Quantum-confinement-induced $\Gamma \rightarrow X$ transition in GaAs/AlGaAs quantum films, wires, and dots

Alberto Franceschetti and Alex Zunger
National Renewable Energy Laboratory, Golden, Colorado 80401
(Received 26 April 1995)

Large GaAs domains embedded in an $Al_xGa_{1-x}As$ matrix act as potential wells for both electrons and holes, resulting in a direct band-gap system. When the GaAs domains become small, however, quantum-confinement effects may push the Γ-like conduction-band state localized on GaAs above the X-like conduction-band state of the $Al_xGa_{1-x}As$ alloy, leading to an indirect band-gap system. Using a pseudopotential band-structure method, as well as the conventional one-band effective-mass approximation, we investigate the nature of the direct→indirect ($\Gamma \rightarrow X$) transition in GaAs/$Al_xGa_{1-x}As$ quantum films, wires, and dots. In the case of an *isolated* GaAs quantum structure embedded in AlAs, we find that the critical size for the onset of the $\Gamma \rightarrow X$ transition increases from ~31 Å in a two-dimensional film through ~56 Å in a one-dimensional cylindrical wire to ~80 Å in a zero-dimensional spherical dot. The interaction between GaAs quantum structures tends to *reduce* the critical size for the $\Gamma \rightarrow X$ transition. We further study the effect of the alloy composition on the $\Gamma \rightarrow X$ transition, finding that the critical size *decreases* when the Ga concentration of the alloy *increases*. In the case of spherical GaAs quantum dots embedded in an $Al_xGa_{1-x}As$ alloy, we show that, as a function of the dot radius and the alloy composition, different alignments of the band-edge states lead to different regimes of the lowest-energy optical transition.

I. INTRODUCTION

Equal-period $(GaAs)_n/(AlAs)_n$ (001) superlattices are known to undergo a type-II→type-I transition[1,2] around the critical period $n_c \sim 11$ monolayers (ML) where the conduction-band minimum (CBM) of the system changes its character from AlAs X-like for $n < n_c$ to GaAs Γ-like for $n > n_c$. This type-II→type-I transition, however, is not restricted to periodic GaAs/AlAs superlattices, but will also occur in GaAs quantum structures embedded in an $Al_xGa_{1-x}As$ matrix. The $Al_xGa_{1-x}As$ alloy is characterized by a critical concentration $x_0 \sim 0.4$ that determines the crossover from a Γ-like direct band-gap semiconductor ($x < x_0$) to an X-like indirect band-gap semiconductor ($x > x_0$). While domains of pure GaAs in a disordered $Al_xGa_{1-x}As$ alloy always act as potential wells for both electrons and holes, the ultimate effect of this attractive potential depends on (i) the size, shape, and distribution of the GaAs domains, (ii) the Al concentration x in the $Al_xGa_{1-x}As$ barrier, and (iii) the presence of external fields, such as electric fields or pressure. When the GaAs domains are sufficiently *large,* both electrons and holes will localize in the GaAs potential wells, resulting in a direct type-I material with Γ-like band-edge states. When the GaAs domains are *small,* however, quantum-confinement effects may push the Γ-like CBM of GaAs above the X-like CBM of the $Al_xGa_{1-x}As$ alloy (for $x > x_0$), leading to an indirect type-II material with an X-like CBM. This mechanism, illustrated in Fig. 1 for the $x=1$ case, is responsible for the quantum-confinement-driven $\Gamma \rightarrow X$ transition in GaAs/$Al_xGa_{1-x}As$ quantum structures. This transition corresponds to a type-I→type-II crossover of the wave-function amplitude in real space, whereby the electron localization shifts from the GaAs quantum structure to the $Al_xGa_{1-x}As$ matrix. Thus, the type-I→type-II crossover provides a lower bound to the size of GaAs nanostructures containing localized electrons. This transition should be observable experimentally as a quenching of the photoluminescence intensity.

In this work we compare the critical sizes for the occurrence of the quantum-confinement-induced $\Gamma \rightarrow X$ transition in GaAs quantum films, wires, and dots, using a pseudopotential band-structure method, as well as a conventional one-band effective-mass approach. We consider simple geometries for the GaAs quantum struc-

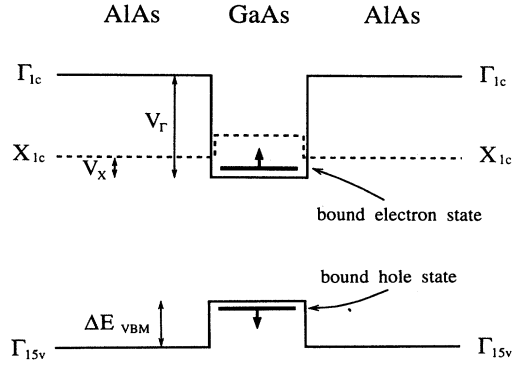

FIG. 1. Band alignment of the GaAs/AlAs heterostructure. The thick solid lines represent bound states localized in the GaAs well. Quantum-confinement effects can push the electron state up, as indicated by the thick arrow, exposing the X_{1c} state of AlAs as the conduction-band minimum. The X_{1c} and L_{1c} levels of GaAs are higher in energy than the X_{1c} level of AlAs by 0.25 and 0.08 eV, respectively. V_Γ and V_X denote the Γ_{1c} and X_{1c} potential barriers, while ΔE_{VBM} is the valence-band offset.

0163-1829/95/52(20)/14664(7)/$06.00

tures: two-dimensional films, one-dimensional cylindrical wires, and zero-dimensional spherical dots; all of these cases are accessible to analytic treatment in the effective-mass framework. In the case of an isolated GaAs quantum structure embedded in AlAs, we find that the critical size for the onset of the $\Gamma \rightarrow X$ transition is 31 Å in a two-dimensional quantum film, 56 Å in a one-dimensional cylindrical quantum wire, and 80 Å in a zero-dimensional spherical quantum dot. We also find that the interaction between GaAs quantum structures tends to *reduce* the critical size for the occurrence of the $\Gamma \rightarrow X$ transition. We further investigate the effects of the alloy composition, finding that the critical size decreases when the Ga concentration in the $Al_xGa_{1-x}As$ matrix increases. This is explained by the reduction of the potential barrier at the GaAs/$Al_xGa_{1-x}As$ interface. In the case of a spherical GaAs quantum dot embedded in $Al_xGa_{1-x}As$, we show that, depending on the dot radius and the alloy composition, different alignments of the band-edge states lead to different regimes of the lowest-energy optical transition.

II. PSEUDOPOTENTIAL CALCULATIONS

A. Method

The pseudopotential method, providing a microscopic description of the system, allows a straightforward identification of the $\Gamma \rightarrow X$ transition in GaAs/AlAs quantum structures. The total pseudopotential (ps) of the system is given by the sum of screened atomic pseudopotentials centered at the atomic positions $\mathbf{R}_n$:

$$V_{\rm ps}(\mathbf{r}) = \sum_n v_n(\mathbf{r}-\mathbf{R}_n) \ . \tag{1}$$

We have used the empirical atomic pseudopotentials developed by Mäder and Zunger,[3] fitted to *measured* interband transition energies, effective masses, and deformation potentials of bulk GaAs and AlAs and to *first-principles* wave functions and level splittings of GaAs/AlAs short-period superlattices. In this approach, the atomic pseudopotential v_n depends not only on the chemical identity of atom n at site $\mathbf{R}_n$, but also on the identity of its nearest neighbors. Note that unlike the one-band effective-mass approximation and the eight-band $\mathbf{k}\cdot\mathbf{p}$ envelope-function approximation,[4] our pseudopotential approach is not restricted to parabolic bands near Γ, and allows coupling between all bulk bands.

Since the systems considered here contain hundreds or even thousands of atoms, conventional diagonalization techniques are not practical for solving the eigenvalue problem. Instead, the band-edge states of the GaAs/AlAs quantum structures are obtained using the folded spectrum method,[5] which searches for the ground state of the operator $(\hat{H}-E_{\rm ref})^2$, where $\hat{H} = -\frac{1}{2}\nabla^2 + V_{\rm ps}(\mathbf{r})$ is the pseudo-Hamiltonian of the system (in atomic units) and $E_{\rm ref}$ is an arbitrary reference energy. The ground state of this operator is the eigenstate of $\hat{H}$ closest in energy to the reference level $E_{\rm ref}$; by choosing $E_{\rm ref}$ in the band gap, one obtains the band-edge states of the system, with the same accuracy achieved in a conventional diagonalization of the Hamiltonian. Since only the band-edge states are obtained, the computational

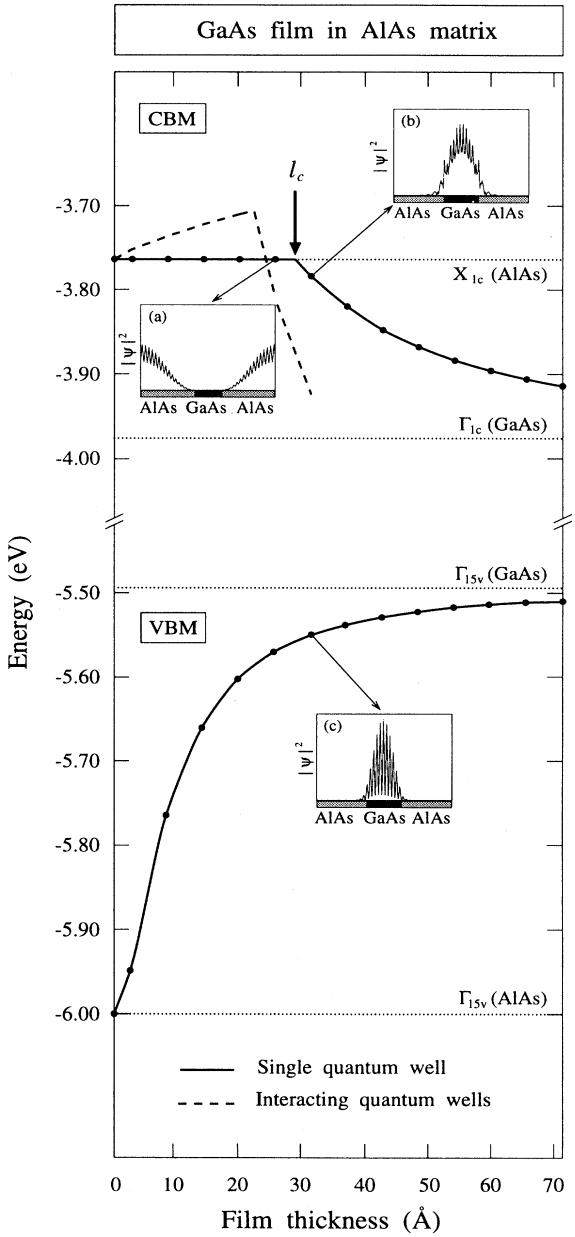

FIG. 2. The VBM and CBM energies of an isolated GaAs quantum film embedded in an AlAs matrix, calculated with the pseudopotential method, are shown as a function of the film thickness (solid dots connected by line). The critical thickness for the $\Gamma \rightarrow X$ transition (l_c) is indicated by a thick arrow. The CBM energy of a periodic array of GaAs films in AlAs is also shown (dashed line); the period of the array is $L=34$ Å. The dotted lines correspond to the energies of the Γ_{15v} and Γ_{1c} states of bulk GaAs and of the Γ_{15v} and X_{1c} states of bulk AlAs. Insets (a) and (b) show the wave-function amplitude of the CBM, averaged over the (001) planes, before and after the $\Gamma \rightarrow X$ transition. Inset (c) shows the wave-function amplitude of the VBM, averaged over the (001) planes.

effort scales linearly with the size of the system. The minimization procedure is carried out in a plane-wave basis set using a preconditioned conjugate-gradients algorithm. Periodic boundary conditions are assumed at the boundaries of a large supercell including the GaAs domain and the AlAs barrier. Because of the use of periodic boundary conditions, a residual interaction between the GaAs domains is inevitable. However, with the choice of a sufficiently thick barrier the convergence of the band-edge energies to the limit of isolated structures is of the order of a few meV.

B. Isolated GaAs quantum structures in pure AlAs

First we consider an isolated (001) GaAs quantum film in an AlAs matrix. Our pseudopotential results are shown in Fig. 2 as a function of the film thickness l. For GaAs films with thickness $l < l_c$ (where $l_c \simeq 28$ Å, or 10 ML's), the CBM energy of the heterostructure is almost degenerate with the X_{1c} energy level of bulk AlAs. An analysis of the CBM wave function for $l < l_c$ shows that this is actually an X-like state localized in the AlAs barrier [insert (a) to Fig. 2]. For thicker GaAs films ($l > l_c$) the CBM energy begins to drop as the film thickness increases, approaching the Γ_{1c} level of bulk GaAs. In this region the CBM wave function has a strong Γ-like character, and is localized in the GaAs film [insert (b) to Fig. 2]. Thus, the $\Gamma \rightarrow X$ crossover is predicted to occur at the critical thickness $l_c \simeq 28$ Å, corresponding to 10 ML of GaAs. The $\Gamma \rightarrow X$ transition is characterized by a dramatic shift in the CBM wave-function localization, as illustrated in the insets of Fig. 2. Since the valence-band maximum (VBM) always has a larger amplitude on the GaAs film [insert (c) to Fig. 2], the $\Gamma \rightarrow X$ transition corresponds to a type-I$\rightarrow$type-II crossover in real space.

A similar pseudopotential calculation has been performed for GaAs cylindrical quantum wires with the axis oriented along the [001] direction. The GaAs/AlAs systems considered in this case contain up to 2304 atoms. The Ga atoms occupy the cation-sublattice positions closer than a given distance (the wire "radius") to the wire axis. The VBM and CBM energies are plotted in Fig. 3 as a function of the wire diameter. Again, thin quantum wires are characterized by an X-like CBM localized in the AlAs barrier, while thick wires have a Γ-like CBM localized on the interior of the GaAs wire, as demonstrated by the insets of Fig. 3. The crossover diameter is found to be $d_c \simeq 52$ Å, which is nearly twice the critical thickness $l_c \simeq 28$ Å for a two-dimensional quantum film. To illustrate the type-I$\rightarrow$type-II crossover, the VBM and CBM wave-function amplitudes are shown in Fig. 4 for GaAs quantum wires of diameter $d = 45.3$ Å and 56.6 Å. When $d < d_c$ the CBM consists of two degenerate X-like states (denoted by "CBM 1" and "CBM 2" in Fig. 4) localized in the AlAs barrier. When $d > d_c$, the CBM is a nondegenerate Γ-like state localized in the GaAs quantum wire.

In the case of a spherical GaAs quantum dot embedded in AlAs the $\Gamma \rightarrow X$ transition diameter is expected to be $\simeq$ 80 Å from a simple effective-mass calculation (see

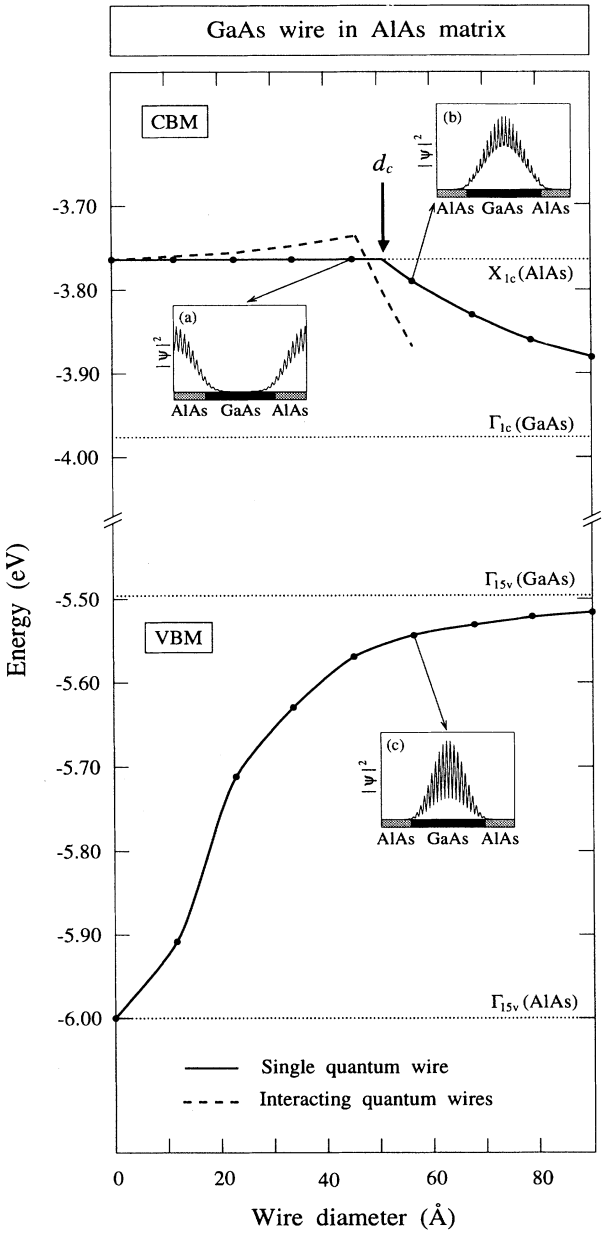

FIG. 3. The VBM and CBM energies of an isolated GaAs cylindrical quantum wire embedded in an AlAs matrix, calculated with the pseudopotential method, are shown as a function of the wire diameter (solid dots connected by line). The critical diameter for the $\Gamma \rightarrow X$ transition (d_c) is indicated by a thick arrow. The CBM energy of a periodic square array of GaAs wires in AlAs is also shown (dashed line); the period of the array is $D = 57$ Å. The dotted lines correspond to the energies of the Γ_{15v} and Γ_{1c} states of bulk GaAs and of the Γ_{15v} and X_{1c} states of bulk AlAs. Insets (a) and (b) show the wave-function amplitude of the CBM before and after the $\Gamma \rightarrow X$ transition; the CBM amplitude, averaged over the (100) planes (parallel to the wire direction), is plotted along the [100] direction. Inset (c) shows the VBM wave-function amplitude along the [100] direction.

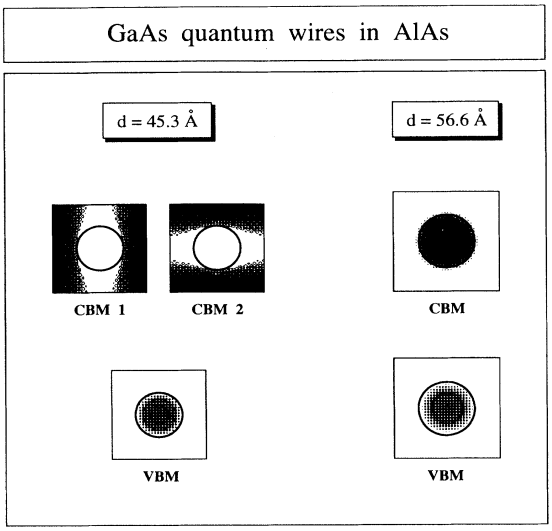

FIG. 4. VBM and CBM wave-function amplitudes of GaAs [001] quantum wires in AlAs. The wave-function amplitude, averaged along the wire direction, is plotted in the (001) plane. The solid circles denote cross sections of the GaAs wires (of diameter d). For $d=45.3$ Å the CBM is a double-degenerate X-like state localized in the AlAs matrix. For $d=56.6$ Å the CBM is a nondegenerate Γ-like state localized in the GaAs wire. In both cases the VBM is localized in the GaAs wire.

next section). Taking into account the thickness of the AlAs barrier necessary to decouple the quantum dots, we estimate the size of the GaAs/AlAs system necessary to observe the $\Gamma \rightarrow X$ transition to be of the order of $\sim 5 \times 10^4$ atoms. This is outside the range accessible to pseudopotential calculations. A recently developed multiband $\mathbf{k}\cdot\mathbf{p}$ method[6] predicts a critical diameter $d_c \simeq 70$ Å for the $\Gamma \rightarrow X$ transition in GaAs/AlAs quantum dots.

C. Interacting GaAs quantum structures in AlAs

To address the consequences of the interaction among GaAs quantum structures for the onset of the $\Gamma \rightarrow X$ transition, we have performed pseudopotential calculations for *interacting* quantum films and quantum wires. First, we consider a periodic array of (001) GaAs quantum films embedded in AlAs (GaAs/AlAs superlattice). The array period (i.e., the distance between the central planes of two consecutive GaAs films) is kept fixed at a value L slightly larger than the transition thickness l_c of a single quantum film, while the well thickness is varied from 0 to L. The results for $L=34$ Å are shown in Fig. 2 (dashed line) as a function of the film thickness l. In comparison to the case of an isolated GaAs quantum film in AlAs, two new effects arise: (i) for thin GaAs films the CBM energy is no longer constant, but initially *increases* with the film thickness, and (ii) for thick GaAs films the CBM energy decreases *faster* than in the case of an isolated film. Thus, the $\Gamma \rightarrow X$ crossover (identified by the change of slope of the dashed line) occurs at a thickness *smaller* than the critical value l_c for an isolated film; of course, the exact value of the critical thickness depends on the array period L.

Similar results are obtained for interacting quantum wires. In this case we have considered a square array of [001]-oriented GaAs cylindrical wires embedded in an AlAs matrix. The CBM energy shown in Fig. 3 (dashed line) is obtained for a nearest-neighbor distance $D=57$ Å.

The reduction of the critical size for the $\Gamma \rightarrow X$ transition can be readily interpreted in the framework of the effective-mass approximation. As we can see from Fig. 1, the X_{1c} state of bulk GaAs is higher in energy than the X_{1c} state of bulk AlAs, so the former acts as a potential barrier for the latter. Thus, when the thickness of the AlAs barrier is finite, the X_{1c} state is pushed up by quantum confinement. Furthermore, electrons bound to neighboring GaAs quantum structures can interact, lowering the ground-state energy, if the barrier is not too thick. These two effects add up to *decrease* the critical size for the onset of the $\Gamma \rightarrow X$ transition.

III. EFFECTIVE-MASS CALCULATIONS

While pseudopotential band-structure calculations provide an accurate, microscopic method to obtain the critical size for the $\Gamma \rightarrow X$ transition, they are not practical when the critical size is very large, such as in GaAs/$Al_xGa_{1-x}As$ quantum dots. For simple domain geometries, on the other hand, the one-band effective-mass approximation (EMA) provides a direct, analytic method for calculating the transition size of GaAs quantum structures embedded in an $Al_xGa_{1-x}As$ barrier. Our basic assumption is that an electron localized in a GaAs domain is confined by a potential barrier V_Γ corresponding to the energy difference between the Γ_{1c} states of $Al_xGa_{1-x}As$ and GaAs (see Fig. 1 for the $x=1$ case). In other words, we neglect the Γ-X mixing of the conduction-band minimum when the latter is localized in GaAs domains. The Schrödinger equation in the EMA is solved by assuming the continuity of the envelope function and of the current density at the boundary of the quantum structure. The critical size for the $\Gamma \rightarrow X$ transition is obtained by equating the confinement energy of the electron to the energy difference V_X between the X_{1c} state of $Al_xGa_{1-x}As$ and the Γ_{1c} state of GaAs (see Fig. 1). At low Al concentrations ($x < x_0$) the alloy band gap is *direct* ($V_\Gamma < V_X$), and the $\Gamma \rightarrow X$ transition of the CBM is not possible. At high Al concentrations ($x > x_0$) the alloy band gap is *indirect* ($V_\Gamma > V_X$), and the $\Gamma \rightarrow X$ transition becomes possible. The details of the EMA calculations are given in the Appendix.

The critical sizes for the $\Gamma \rightarrow X$ transition in GaAs quantum films, wires, and dots, calculated using the parameters[7–9] given in Table I, are plotted in Fig. 5 against the Al concentration x in the $Al_xGa_{1-x}As$ barrier. In the case of GaAs quantum films, we show the critical thickness l_c, while for wires and dots we show the critical diameter d_c. As we can see, the $\Gamma \rightarrow X$ transition size increases monotonically with the Al concentration, and decreases with the dimensionality of the system: $d_c(\text{dot}) > d_c(\text{wire}) > l_c(\text{film})$. This is so because the critical size increases when the confinement effects increase. In

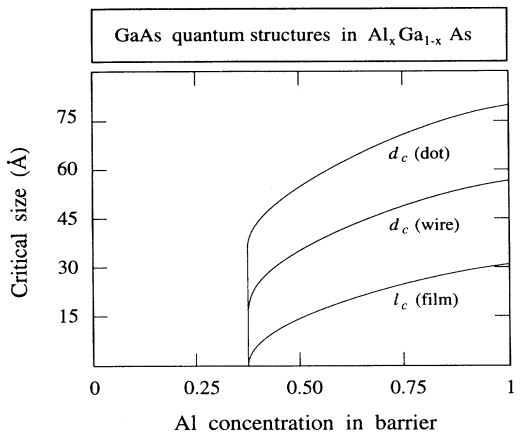

FIG. 5. Critical size for the $\Gamma \rightarrow X$ transition in $GaAs/Al_xGa_{1-x}As$ quantum films, wires, and dots, as a function of the Al concentration in the barrier, calculated by the effective-mass approximation.

the case $x=1$, we obtain $l_c \simeq 31$ Å for a quantum film and $d_c \simeq 56$ Å for a cylindrical quantum wire. These results should be compared with $l_c \simeq 28$ Å and $d_c \simeq 52$ Å obtained from the pseudopotential calculations: the difference is less than 10%, suggesting that *in this size regime* the EMA is a good approximation.

A detailed discussion of the applicability of the EMA to heterostructures can be found in Ref. 10. Mäder and Zunger[11] recently compared the one-band EMA with direct pseudopotentials calculations for $(GaAs)_n/(AlAs)_n$ (001) superlattices, and Wood and Zunger[12] presented a similar comparison for the eight-band $\mathbf{k}\cdot\mathbf{p}$ model. It was found that both the one-band EMA and the eight-band $\mathbf{k}\cdot\mathbf{p}$ model miss some important features obtained by the direct diagonalization in *short-period superlattices,* namely, the reduction of the Γ-folded conduction state as the period n is decreased below $n=3$ and the even-odd oscillations of the L-folded conduction state below $n=8$.

TABLE I. Material parameters for bulk GaAs and AlAs and for the $Al_xGa_{1-x}As$ alloy used in the effective-mass calculations. Here m is the Γ_{1c} effective mass, E_Γ and E_X are the Γ_{1c} and X_{1c} band gaps, b_Γ and b_X are the alloy bowing parameters for the Γ_{1c} and X_{1c} band gaps, and ΔE_{VBM} is the valence-band offset of the GaAs/AlAs heterojunction.

Parameter	GaAs		AlAs
m (m_0)	0.067[a]		0.154[a]
E_Γ (eV)	1.52[a]		3.13[a]
E_X (eV)	1.98[a]		2.23[a]
b_Γ (eV)		$0.58+1.06(x-0.5)$[b]	
b_X (eV)		0.245[a]	
ΔE_{VBM} (eV)		0.50[c]	

[a]Reference 7.
[b]Reference 8.
[c]Reference 9.

In Fig. 6 we show the size vs composition (d-x) "phase diagram" of a single GaAs quantum dot of diameter d embedded in the $Al_xGa_{1-x}As$ alloy. The critical radius for the $\Gamma \rightarrow X$ transition (solid line) and the minimum size needed to localize an electron in the GaAs quantum dot when $x < x_0$ (dotted line) are plotted as a function of the Al concentration in the barrier. The EMA also predicts a minimum size for the localization of the hole in the GaAs quantum dot; due to the large effective mass of the hole, however, the corresponding wave function is expected to have a strong resonance on the GaAs quantum dot even below this minimum size. As a result, the d-x plane can be divided into three regions, corresponding to different band-gap alignments of the $GaAs/Al_xGa_{1-x}As$ heterostructure. In region I the CBM is a Γ-like state localized in the GaAs quantum dot. Since the valence-band maximum is also a Γ-like state localized mainly in the GaAs quantum dot, the lowest-energy optical transition is direct both in real space and in reciprocal space (type-I arrangement). In region II the CBM is an X-like state localized in the $Al_xGa_{1-x}As$ barrier, and the band gap is indirect both in real space and in reciprocal space (type-II arrangement). Finally, in region III the Γ-like CBM is delocalized over the whole system, although it may have a strong resonance on the GaAs quantum dot. The results of Fig. 6 may be relevant to the discussion of phase separation in alloys. We see from the figure that when an otherwise homogeneous, indirect $Al_xGa_{1-x}As$ alloy begins to phase separate into GaAs-rich and AlAs-rich domains, the system will have a direct band gap if the GaAs clusters are in the size range of region I in Fig. 6.

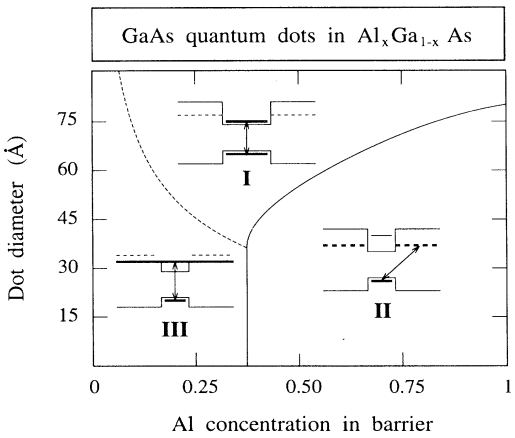

FIG. 6. d-x "phase diagram" of a GaAs spherical quantum dot of diameter d embedded in an $Al_xGa_{1-x}As$ matrix. The three regions denoted by I, II, and III correspond to different alignments of the band-edge states. As shown by the insets, in region I the lowest-energy optical transition, denoted by an arrow, occurs between bound states localized in the GaAs quantum dot; in region II the lowest-energy optical transition is indirect, with the hole localized in the GaAs quantum dot and the electron localized in the $Al_xGa_{1-x}As$ barrier; finally, in region III the electron is in a delocalized Γ-like state with a resonance in the GaAs quantum dot.

IV. SUMMARY

In conclusion, we have shown that both the pseudopotential band-structure method and the effective-mass approximation provide useful information about the $\Gamma \rightarrow X$ transition in thin GaAs quantum structures embedded in an $Al_xGa_{1-x}As$ matrix and the related type-I $\rightarrow$ type-II crossover in the probability distribution of the band-edge wave functions. We have found that the critical size for the $\Gamma \rightarrow X$ transition increases when the dimensionality of the system decreases, and that the interaction between GaAs quantum structures tends to reduce the critical size. We have also discussed the effects of the alloy composition on the $\Gamma \rightarrow X$ transition, finding that for a $GaAs/Al_xGa_{1-x}As$ spherical quantum dot three different regimes for the character of the lowest-energy optical transition can be identified as a function of the dot diameter and the alloy composition. Although the size of the $GaAs/Al_xGa_{1-x}As$ quantum dots that can be currently fabricated is larger than the critical size for the $\Gamma \rightarrow X$ transition, recent progress in nanotechnology can lead to the realization of nanostructures with a typical size smaller than 100 Å, making the observation of this transition possible.

ACKNOWLEDGMENTS

The authors are grateful to Kurt Mäder, Lin-Wang Wang, and David Wood for useful discussions. This work was supported by the U.S. Department of Energy, Office of Energy Research, Basic Energy Science, Division of Materials Science, under Grant No. DE-AC36-83CH10093.

APPENDIX: EMA CALCULATION OF THE CRITICAL SIZE FOR THE $\Gamma \rightarrow X$ TRANSITION

The critical size for the $\Gamma \rightarrow X$ transition in $GaAs/Al_xGa_{1-x}As$ quantum structures can be calculated directly within the effective-mass approximation. The potential barriers V_Γ and V_X (Fig. 1) depend on the Al concentration x in the alloy. They are calculated as

$$V_\Gamma(x)=E_\Gamma(Al_xGa_{1-x}As)-E_\Gamma(GaAs) -\Delta E_{VBM}(x) \quad (A1)$$

and

$$V_X(x)=E_X(Al_xGa_{1-x}As)-E_\Gamma(GaAs) -\Delta E_{VBM}(x) , \quad (A2)$$

where E_Γ and E_X are the Γ_{1c} and X_{1c} energy gaps, respectively, and $\Delta E_{VBM}(x)$ is the x-dependent valence-band offset between GaAs and the $Al_xGa_{1-x}As$ alloy. The energy gaps of the alloy depend quadratically on x via the bowing parameters b_Γ and b_X:

$$E_\Gamma(Al_xGa_{1-x}As)=E_\Gamma(GaAs) +x[E_\Gamma(AlAs)-E_\Gamma(GaAs)] -b_\Gamma x(1-x) , \quad (A3)$$

$$E_X(Al_xGa_{1-x}As)=E_X(GaAs) +x[E_X(AlAs)-E_X(GaAs)] -b_X x(1-x) , \quad (A4)$$

while a linear composition dependence is assumed for the valence-band offset. In the following, we will denote by m_w the electron effective mass of the GaAs well (w) and by m_b the x-dependent electron effective mass of the $Al_xGa_{1-x}As$ barrier (b) at the Γ point; the latter is obtained by linear interpolation of the effective masses of pure AlAs and GaAs:

$$m_b(x)=m_{GaAs}+x(m_{AlAs}-m_{GaAs}) . \quad (A5)$$

We will also use the notation $k_w=(2m_wV_X)^{1/2}$ and $k_b=[2m_b(V_\Gamma-V_X)]^{1/2}$, where atomic units are assumed. The parameters used in the EMA calculations are summarized in Table I; these parameters yield a value $x_0=0.372$ for the direct/indirect transition of the $Al_xGa_{1-x}As$ alloy, compared to the experimental value[7] $x_0=0.43$.

In the case of a quantum film, the critical thickness for the $\Gamma \rightarrow X$ transition can be obtained explicitly as

$$l_c=\frac{2}{k_w}\arctan\left[\frac{m_w}{m_b}\frac{k_b}{k_w}\right] . \quad (A6)$$

Note that the arctan function is multiple valued; the only value of interest in this context is the lowest positive one. The remaining positive solutions give the localization thickness of higher-energy states with the same parity as the ground state. For a cylindrical quantum wire, the transition radius r_c is given by the lowest positive solution of the following equation:

$$\frac{k_w}{m_w}\frac{J_1(k_wr_c)}{J_0(k_wr_c)}=\frac{k_b}{m_b}\frac{K_1(k_br_c)}{K_0(k_br_c)} , \quad (A7)$$

where J_n and K_n are the nth-order ordinary and modified Bessel functions, respectively. Finally, in the case of a spherical quantum dot the transition radius r_c is given by the lowest positive solution of the following equation:

$$\frac{k_wr_c}{\tan(k_wr_c)}=1-\frac{m_w}{m_b}(1+k_br_c) . \quad (A8)$$

A comment about the case $x=x_0$ (i.e., $V_\Gamma=V_X$) is in order at this point. When $x \rightarrow x_0^+$ we have $k_b \rightarrow 0^+$, and thus from Eqs. (A6) and (A7) we obtain $l_c \rightarrow 0$ and $r_c \rightarrow 0$, respectively. An inspection of Eq. (A8), however, shows that for a spherical dot one has $r_c > 0$ even when $k_b \rightarrow 0^+$. This is a consequence of the well-known fact that a square potential well will always bind at least one state in one and two dimensions, no matter how shallow the potential well, while this is not the case in three dimensions.

[1]A. Ishibashi, Y. Mori, M. Itabashi, and M. Watanabe J. Appl. Phys. **58**, 2691 (1985); G. Danan, B. Etienne, F. Mollot, R. Planel, A. M. Jean-Louis, F. Alexandre, B. Jusserand, G. Le Roux, J. Y. Marzin, H. Savary, and B. Sermage, Phys. Rev. B **35**, 6207 (1987); G. Li, D. Jiang, Z. Wang, and K. Ploog, *ibid.* **40**, 10430 (1989).

[2]W. Ge *et al.*, J. Lumin. **59**, 163 (1994).

[3]K. A. Mäder and A. Zunger, Phys. Rev. B **50**, 17393 (1994).

[4]G. Bastard, Phys. Rev. B **24**, 5693 (1981); G. A. Baraff and D. Gershoni, *ibid.* **43**, 4011 (1991).

[5]L.-W. Wang and A. Zunger, J. Chem. Phys. **100**, 2394 (1994).

[6]L.-W. Wang and A. Zunger (unpublished).

[7]*Semiconductors. Physics of Group IV Elements and III-V Compounds,* edited by O. Madelung, M. Schulz, and H. Weiss, Landolt-Börnstein, New Series, Group III, Vol. 17, Pt. a (Springer, Berlin, 1982).

[8]S.-H. Wei and A. Zunger, Phys. Rev. B **39**, 3279 (1989).

[9]J. Wolford, in *Physics of Semiconductors: Proceedings of the 18th International Conference, Stockholm, 1986,* edited by O. Engström (World Scientific, Singapore, 1987), p. 1115.

[10]M. G. Burt, J. Phys. Condens. Matter **4**, 6651 (1992).

[11]K. A. Mäder and A. Zunger, Europhys. Lett. **31**, 107 (1995).

[12]D. M. Wood and A. Zunger (unpublished).